Available online at www.sciencedirect.com
ScienceDirect
Journal of Power Sources 180 (2008) 664–670
JOURNAL OF POWER SOURCES
www.elsevier.com/locate/jpowsour

Electrochemical properties of nanosized hydrous manganese dioxide synthesized by a self-reacting microemulsion method

Chengjun Xu [a,b], Baohua Li [a], Hongda Du [a], Feiyu Kang [b,*], Yuqun Zeng [c]

[a] *Advanced Materials Institute, Graduate School at Shenzhen, Tsinghua University, Shenzhen City, Guangdong, 518055, China*
[b] *Department of Materials Science and Engineering, Tsinghua University, Beijing, 100084, China*
[c] *Amperex Technology Limited, Dongguan City, Guangdong, 523080, China*

Received 26 October 2007; received in revised form 28 December 2007; accepted 1 February 2008
Available online 10 March 2008

Abstract

Manganese dioxide has been synthesized by a new simple self-reacting microemulsion method. The synthesized MnO_2 has been found to be amorphous structure containing a moderate amount of water by X-ray diffraction, Fourier transform infrared spectroscopy and thermogravimetric analysis. Particles in a spherical shape with about 4 nm in diameter have been observed by transmission electron microscopy. Cyclic voltammetic tests have been performed between −0.5 and 0.5 V versus Hg/Hg_2SO_4 in 1 mol L^{-1} Na_2SO_4 solution at sweep rates up to 50 mV s^{-1}. A specific capacitance value as high as 246.2 F g^{-1} was obtained, which was much higher than 146.5 F g^{-1} of MnO_2 prepared by chemical co-precipitation. After 600 cycles, only 6% decrease of specific capacitance was measured which indicated that such a material possesses good cycling property.

Keywords: Manganese dioxide; Self-reacting microemulsion; Pseudo-capacitance; Supercapacitor

1. Introduction

Electrochemical supercapacitors can be divided into two types based on the fundamental mechanisms that govern the capacitances. First is based on the electrical double layers in high surface area materials such as activated carbons which have specific surface area in excess of 1000 m^2 g^{-1}. Second is the redox capacitors where a faradic charge exchange occurs leading to the pseudo-capacitance [1]. Many noble or transition metal oxides can show pseudo-capacitive behavior, and among different metal oxides, amorphous hydrous RuO_2 has a high specific capacitance (760 F g^{-1}) in H_2SO_4 solution [2]. However, high cost, low porosity and rapid decrease of power density at high charge–discharge rate are prohibitive to large-scale commercial production. Thus, the suitable materials with good capacities and low cost have attracted much attention. Since Lee and Goodenough first reported the ideal capacitive behavior of hydrous manganese dioxide in mild solutions, more and more attentions have been paid to manganese dioxide because it is inexpensive, its raw materials are abundant, and it is environmentally friendly [3].

Manganese dioxide powders, synthesized by chemical co-precipitation, sol–gel and hydrothermal synthesis, have shown that the average specific capacitance is about 160 F g^{-1} [4–7], which is competitive with carbon supercapacitors, but falls far short of the 760 F g^{-1} obtained with hydrous RuO_2 [2]. Manganese dioxide thin films prepared by dip-coating, anodic deposition or electrochemical oxidation can reach as high as a capacitance of 450 F g^{-1} due to high utilization of material [8–13]. However, this high specific capacitance can only be obtained at a very low loading mass, less than 0.2 mg cm^{-2}. Moreover, only half of this value, 230 F g^{-1}, is left, if loading mass increases to 0.3–0.4 mg cm^{-2} [9–16]. Considering these disadvantages, thin films are limited to microsystems for energy storage such as integrated devices. Industrial application in high-power density devices requires the use of the active material usually mixed with a binder and a conductive additive to prepare composite electrodes [4].

Based on the above points of view, it is more desirable to employ an alternative method to replace the chemical

* Corresponding author. Tel.: +86 10 6277 3752; fax: +86 10 6277 1160.
E-mail address: fykang@tsinghua.edu.cn (F. Kang).

0378-7753/$ – see front matter © 2008 Elsevier B.V. All rights reserved.
doi:10.1016/j.jpowsour.2008.02.029

co-precipitation or sol–gel method for preparing hydrous manganese dioxide powder with excellent capacitive characteristics (i.e. high reversibility, acceptable capacitance and long cycle life) and simple process. Microemulsion is a route for synthesis of nanoparticles of metals and metal oxides. Micro–nano droplets of water phase containing the reactants are dispersed and stabilized by a surfactant in an organic medium, and reactions carried out in microemulsion media will produce nanopaticles [17]. However, it was a complicated, time-consuming and raw materials-wasting method because the emulsion of each reactant must be prepared before synthesis and the surfactants are not involved in reaction.

In this study, we report a simple self-reacting emulsion method for the first time. The nanosized hydrous manganese dioxide was synthesized by one step process, in which surfactant sodium bis(2-ethylhexyl) sulfosuccinate (AOT) was used as both dispersant and reductant. $KMnO_4$ aqueous solution was dispersed in iso-octane by AOT to form nano droplets of water phase, and then $KMnO_4$ was reduced by AOT. The manganese oxide particles were found to possess a spherical shape of about 4 nm in diameter. Electrochemical characterization studies of MnO_2 pertaining to supercapacitor properties were also performed.

2. Experimental

2.1. Preparation of MnO_2

The MnO_2 powder was synthesized by a simple method. A 0.1 mol L^{-1} $KMnO_4$ aqueous solution was prepared by dissolving potassium permanganate (AR, 99%) in deionized water. Meanwhile 13.32 g surfactant of high purity sodium bis(2-ethylhexyl) sulfosuccinate (Aerosol-OT, AOT) was added in 300 mL iso-octane (oil) and stirred well to get an optically transparent AOT/iso-octane solution. Then 32.4 mL of 0.1 mol L^{-1} $KMnO_4$ solution was added in AOT/iso-octane solution, and this solution was dispersed by ultrasound for 30 min to prepare a dark brown precipitate. The product was separated, washed copiously several times with distilled water and ethanol, and dried at 80 °C for 12 h. The sample is denoted as s-MnO_2 for the following tests.

In order to compare the electrochemical properties of as-prepared MnO_2 with conventional synthesis methods, chemical co-precipitation technique was also used to prepare MnO_2. A 0.1 mol L^{-1} $KMnO_4$ solution was prepared by dissolving potassium permanganate (AR, 99%) in deionized water. While stirring the solution, a 0.15 mol L^{-1} $Mn(CH_3COO)_2$ was quickly added. The $KMnO_4$/$Mn(CH_3COO)_2$ molar ratio was 2:3. A dark brown precipitate was immediately obtained according to

$$2Mn(VII) + 3Mn(II) \rightarrow 5Mn(IV) \quad (1)$$

The solution was then stirred for 4 h until the reaction completed. The product was separated, washed copiously several times with double distilled water, and dried at 80 °C for 12 h. The sample is denoted as co-MnO_2.

2.2. Characterization

Thermogravimetric analysis (TGA) and differential scanning calorimetry (DSC) for both samples were recorded in the temperature range from ambient to 600 °C in nitrogen atmosphere at a heating rate of 10 °C per min using Sta449C (Netzsch) tester. Powder X-ray diffraction (XRD) patterns of MnO_2 powders were obtained by using TW3040/60 diffractometer (Tanalygical Company, Holland) in which Cu-Kα was used as the source. Morphology of MnO_2 was examined using scanning electron microscope, SEM (Hitachi, S-5200) and transition electron microscope (TEM) (Jeol JEM2100F). Fourier transform infrared spectroscopy (FT-IR) analysis was carried out by Nicolet Magna-IR 550/560 spectrophotometer and the weight ratio of sample to KBr is 1:500. N_2 adsorption and desorption studies were carried out using ASA P2010 (Micromeritics Company) surface area analyzer.

2.3. Electrochemical measurement

Electrodes were prepared by mixing 70 wt% of MnO_2 powder as active material with 20 wt% acetylene black and 10 wt% polytetrafluoroethylene (PTFE). 70 mg of MnO_2 powder and 20 mg of acetylene black were first mixed and dispersed in ethanol by ultrasound for 30 min. Then the ink was dried at 80 °C for 4 h to get dark mixed powder and 200 mg of PTFE aqueous solution (5 wt%) was added to get a paste. Then the paste was dried at 80 °C and a few of 1-methy-2-pyrrolidinone (NMP) were added to get a syrup. The syrup was cold rolled into thick films. Pieces of film with 5 mg weight, typically 1 cm^2 in size, were then hot-pressed at 80 °C under 100 MPa on a stainless steel mesh connected to a nickel wire.

Electrochemical tests were performed with an Im6e (Zahner) electrochemical station. A piece of platinum gauze and Hg/Hg_2SO_4 (in saturated K_2SO_4) were assembled as the counter and reference electrode. The cyclic voltammetry was carried out in a potential range of −0.5 and 0.5 V (versus Hg/Hg_2SO_4) at sweep rates ranging from 2 to 50 mV s^{-1}. Galvanostatic charge–discharge cycling experiments were performed in a range of current densities from 0.7 to 7 mA cm^{-2}.

In order to determine the contribution of acetylene black to the overall charge capacity of electrode, a cyclic voltammetric experiment was performed on an acetylene black electrode without MnO_2. The charge capacitance of this electrode was found to be negligible (≈10 F g^{-1}).

3. Results and discussion

3.1. Material characteristics

There may be two steps involved in the formation of MnO_2 precipitation. At first the $KMnO_4$ solution (water phase) was dispersed in iso-octane (oil phase) by surfactant AOT to form nano droplets of water phase. $KMnO_4$ is a strong oxidation agent and can easily oxidize sulfonates, thus $KMnO_4$ can be reduced subsequently by AOT to produce MnO_2 precipitation and the

growth of MnO_2 particles was restricted by extra AOT to remain nanoscale.

Surface morphologies of s-MnO_2 and co-MnO_2 are shown in Fig. 1. It can be seen from Fig. 1c and b that co-MnO_2 has a rodlike morphology. The diameter of nanorods is about 12 nm, and the length is about 100 nm. TEM images (Fig. 1a and b) of s-MnO_2 show each particle of s-MnO_2 consists of an agglomeration of small spherical particles with an individual particle size of about 4 nm, which is much smaller than that of co-MnO_2.

TGA and DSC thermograms of s-MnO_2 and co-MnO_2 powders are shown in Fig. 2a and b, respectively. TGA and DSC thermograms of both samples powders show 20% weight loss and endotherm around 100 °C, which correspond to dehydration of the powders. Small weight loss and exotherm around 500 °C could be attributed to the loss of oxygen from MnO_2 lattice resulting in phase transition from MnO_2 to Mn_2O_3 [17,18]. TGA/DSC results show that two types of MnO_2 are hydrous oxides and could be described as $MnO_2{\cdot}H_2O$.

Fig. 3 shows XRD profiles for both samples. They are similar and only a few broad peaks appear. Lack of clear peaks and broadening of peaks indicate the amorphous nature. Broad peaks around $2\theta = 37.0^\circ$ and 65.3° are present, which is similar to the literatures [5,17,19]. It is thus inferred that the samples present in a partially crystalline state and the profiles seem to correspond to some peaks of α-MnO_2 (JCPDS NO. 44-0141).

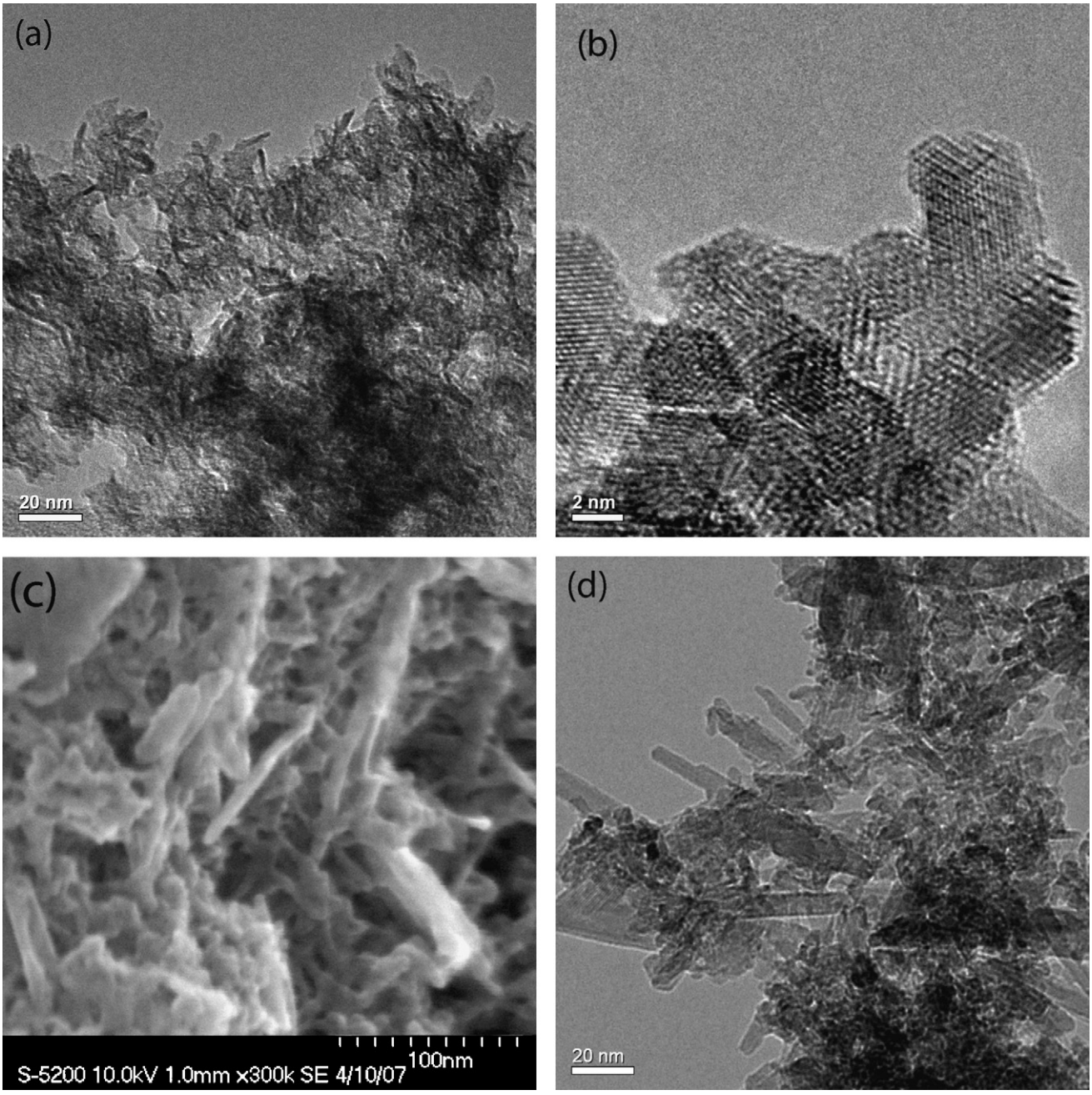

Fig. 1. Surface morphology of (a and b) s-MnO_2 and (c and d) co-MnO_2.

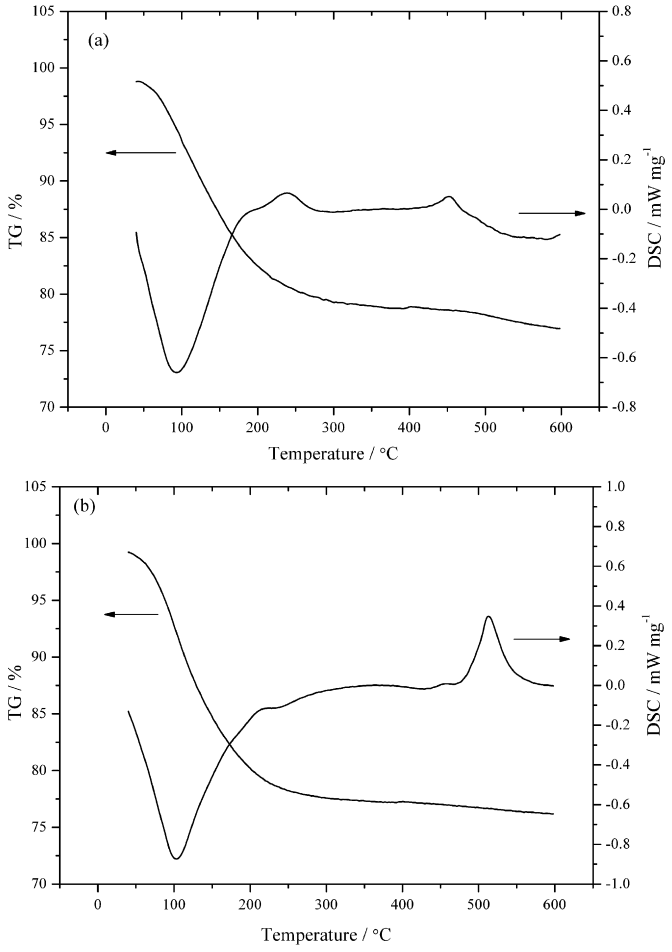

Fig. 2. TGA and DSC curves of (a) s-MnO_2 and (b) co-MnO_2.

N_2 adsorption and desorption studies were performed to determine the specific surface area and the pore size distribution of both samples. S_{BET} values of s-MnO_2 and co-MnO_2 are 145.7 and 217.3 $m^2\,g^{-1}$, respectively. Pore size distribution of s-MnO_2 and co-MnO_2 are shown in Fig. 4. According to IUPAC nomenclature, micropores are less than 2 nm in diameter, mesopores are between 2 and 50 nm in diameter, and macropores are greater than 50 nm in diameter.

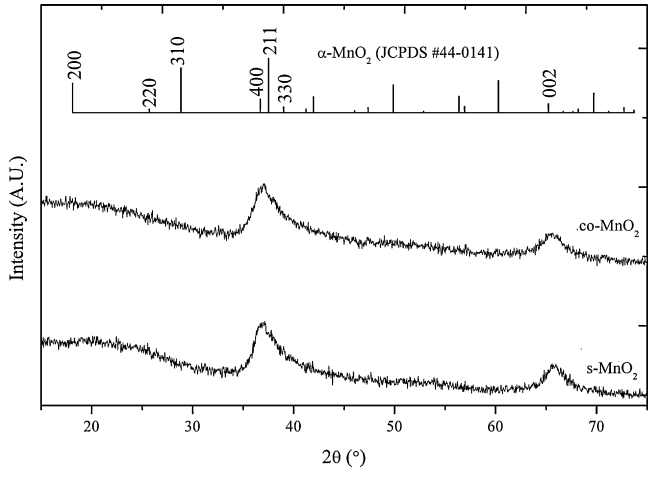

Fig. 3. XRD patterns of s-MnO_2 and co-MnO_2.

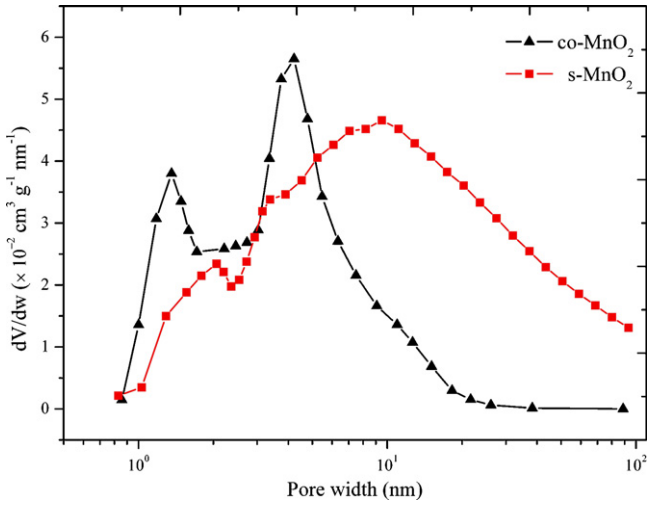

Fig. 4. Pore size distribution of co-MnO_2 and s-MnO_2.

Fig. 4 shows that for s-MnO_2, a very broad distribution ranging from 2 to 100 nm with a mean width around 10 nm is found in the mesopore and macropore region. Moreover, according to the TEM images, the primary particles of s-MnO_2 are about 4 nm in diameter and no pores inside the primary particles were observed. Therefore, it seems that the mesopores and macropores of s-MnO_2 sample come from the pileup of its primary and secondary particles and the specific surface area mainly contributes from the surface of its primary particles. For co-MnO_2, two narrow peaks with mean pore widths of around 1.3 and 4 nm were emerged. Considering the large particle size, it seems that co-MnO_2 possess a porous structure with small pore sizes. It is clear that the high specific surface area of co-MnO_2 mainly contributes from the pores inside the particles.

Physical characterizations indicate that s-MnO_2 and co-MnO_2 possess almost the same crystalline structure, and contain the same water content, but they are quite different in morphology, specific surface area and pore size distribution. A smaller size with spherical shape was obtained for s-MnO_2, as compared with co-MnO_2. Although s-MnO_2 has a smaller S_{BET} value, but it mainly contains architectural mesopores and macropores, and has a wide pore size distribution in the mesopore and macropore region, on the contrary co-MnO_2 seems to be a porous material with small pore sizes and a narrow pore size distribution.

3.2. Electrochemical properties

As-prepared samples were subjected to typical cyclic voltammetric tests in 1 mol L^{-1} Na_2SO_4 solution. The potential range is from −0.5 to 0.5 V versus Hg/Hg_2SO_4 and different scanning rates are taken from 2 to 50 mV s^{-1}. Figs. 5 and 6 show the cyclic voltammograms (CVs) of s-MnO_2 and co-MnO_2, respectively.

These CVs are relatively rectangular in shape and exhibit near mirror-image current response on voltage reversal indicating a reversible reaction and ideal capacitive behavior for both samples. With the increase of scanning rates, there is no signifi-

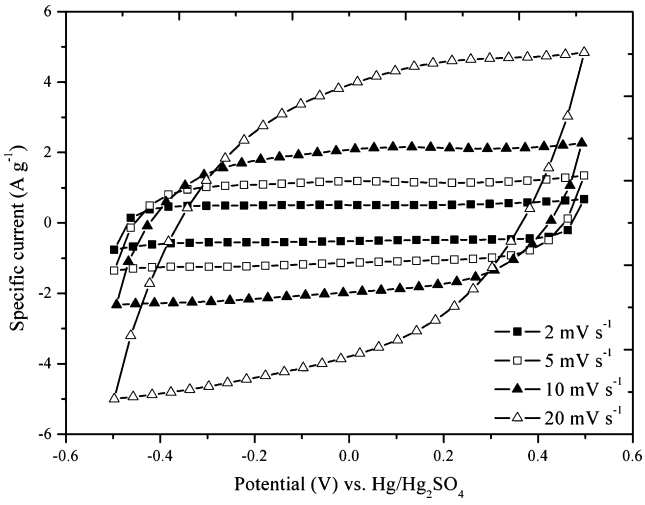

Fig. 5. Cyclic voltammograms of s-MnO_2 at different scanning rates in 1 mol L^{-1} Na_2SO_4.

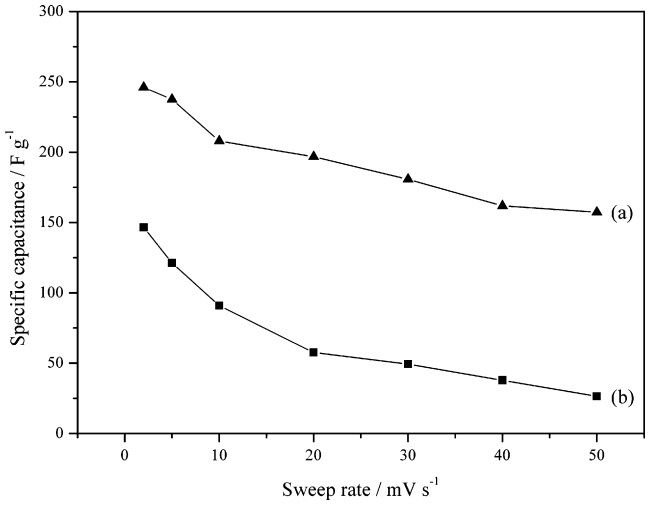

Fig. 7. The dependence of SC for (a) s-MnO_2 and (b) co-MnO_2 on scanning rates.

cant change in rectangular shape exhibiting high electrochemical reversibility in this potential range at high sweep rate. The specific capacitance (SC) of electroactive material can be estimated using half the integrated area of the CV curve to obtain the charge (Q), and subsequently being divided the charge by the mass of the active material (m) and the width of the potential window (ΔV):

$$\mathrm{SC} = \frac{Q}{\Delta V m} \tag{2}$$

Dependence of capacitances calculated from CVs and scanning rates is shown in Fig. 7 for both MnO_2 samples. At a low sweep rate of 2 mV s^{-1}, the SC of s-MnO_2 calculated from CV curve is 246.2 F g^{-1}. At a scanning rate of 50 mV s^{-1}, a high value of 157.3 F $g^{-1}$of s-MnO_2 was obtained, but a very low value of 26.4 F g^{-1} was measured for co-MnO_2, which indicates the s-MnO_2 is a promising electrode material for high-power supercapacitors.

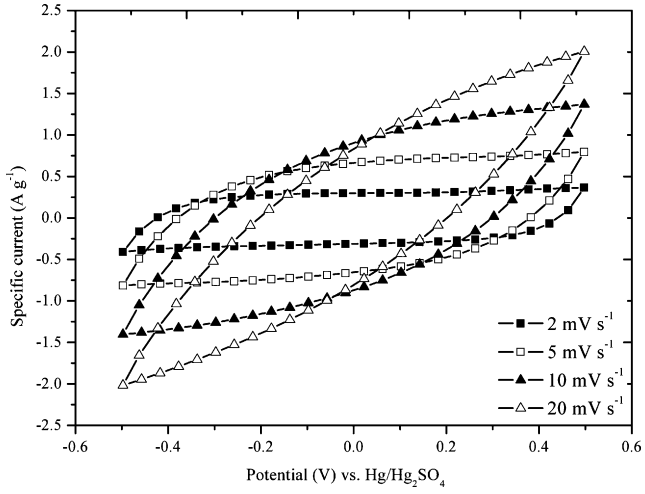

Fig. 6. Cyclic voltammograms of co-MnO_2 at different scanning rates in 1 mol L^{-1} Na_2SO_4.

There are two mechanisms proposed for the charge storage in MnO_2 material. The first one is based on the concept of H^+ or alkali metal cations (C^+) such as Na^+ in this case during reduction and deintercalation upon oxidation. This process is accompanied by the reversible reaction of Mn^{4+}/Mn^{3+}.

$$\mathrm{MnO_2} + \mathrm{C^+} + \mathrm{e^-} \leftrightarrow \mathrm{MnOOC} \tag{3}$$

The second one is the adsorption of cations in the electrolyte on the MnO_2 surface.

$$(\mathrm{MnO_2})_{\mathrm{surface}} + \mathrm{C^+} + \mathrm{e^-} \leftrightarrow (\mathrm{MnO_2{}^-C^+})_{\mathrm{surface}} \tag{4}$$

For hydrous MnO_2, a common viewpoint is that the redox process is mainly governed by the insertion and deinsertion of Na^+ and or H^+ from the electrolyte into nanostructured MnO_2 matrix [4,6]. Increasing the scanning rate will have a direct impact on the diffusion time of cations into matrix leading to the sharp decrease of available capacity.

In order to understand the difference of SC values between two samples, the dependence of voltammetric charge, q, on $v^{-1/2}$ for both samples is shown in Fig. 8a. In Fig. 8b the inverse of the voltammetric charge, q^{-1}, is plotted as a function of square root of sweep rate, $v^{1/2}$.

The method to discriminate the so-called "inner" and "outer" charges was proposed by Trasatti and his co-workers firstly [20]. The whole surface of MnO_2 electrode could be divided into "inner" surface (such as loose grain boundaries, pores inside particles, cracks *etc.*), which is more difficult to access and "outer" surface (such as architectural large mesopores or macropores *etc.*), which is straightforwardly accessible to cations. At high sweep rate, the fast scanning rate will lead to the Na^+ and or H^+ reaching only the "outer" surface of MnO_2 particles that is straightforwardly accessible. Therefore the extrapolation of q to $v = \infty$ from the q versus $v^{-1/2}$ plot (Fig. 8a) gives the "outer" charge of q_0, the charge on the active "outer" surface. The extrapolation of q to $v = 0$ from the q^{-1} versus $v^{1/2}$ plot (Fig. 8b) gives the total charge q_T, which is the charge involved to the whole "inner" and "outer" surfaces of cations [5,7,20,21].

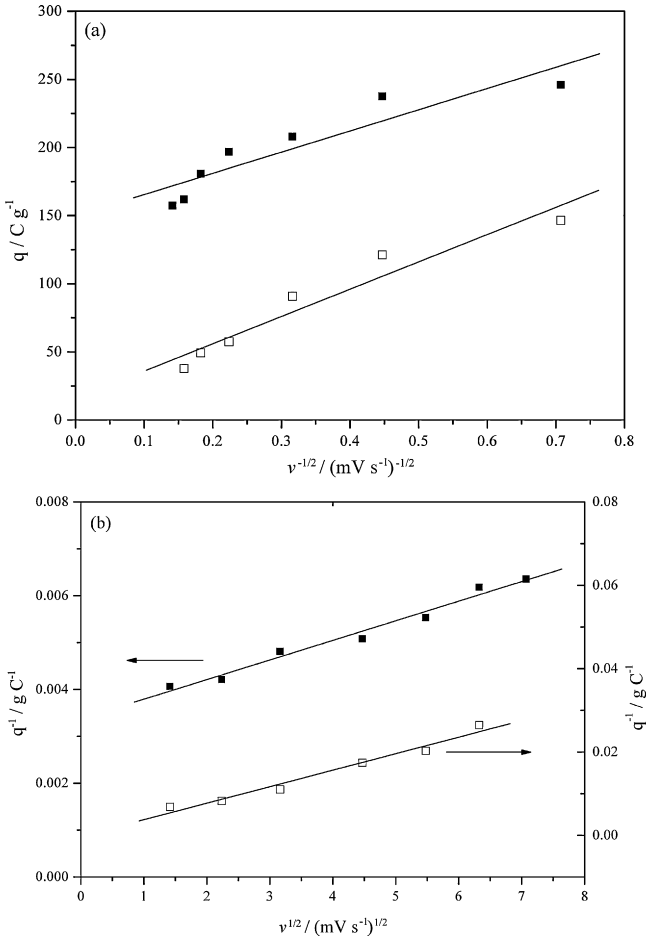

Fig. 8. Variation of the voltammetric density (q) with respect to scanning rate (v): (a) q versus $v^{-1/2}$ plot and (b) q versus $v^{1/2}$ plot for s-MnO_2 (closed square) and co-MnO_2 (open square).

The estimated charges of s-MnO_2 and co-MnO_2 at very low and very high sweep rates are presented in Table 1. The charges of s-MnO_2 and co-MnO_2 at very low scanning rate are 295.2 C g^{-1} and 212.8 C g^{-1}, respectively. A high value of q_0 for s-MnO_2, 156.8 C g^{-1}, is obtained, which indicates most surface of s-MnO_2 are straightforwardly accessible for cations. The real charge, q_r, at 2 mV s^{-1} is also presented in Table 1. The ratio of q_r to q_T may symbolize the utilization of MnO_2 representing the proportion of active material, which is involved in the charge storage process. As high as 83.4% of s-MnO_2 is obtained compared with 68.8% of co-MnO_2.

Previous results of physical characterizations indicate that s-MnO_2 mainly contains architectural mesopores and macropores, but co-MnO_2 is a microporous material with the narrow pore size distribution. It is well know that large pores are advantageous in mass transport and the ions in the electrolyte can transport in the macropores and mesopores more easily and rapidly than in the micropores. For the whole charge storage process of hydrous MnO_2 involving transport and insertion of cations in the electrolyte, large pore size and a wide pore size distribution in the mesopore and macropore region insure most surface of s-MnO_2 are straightforwardly accessible for cations. For co-MnO_2, its small pores inside particles are hardly accessible for cations and lack of macropores may slow down the transport of cations. Therefore a high SC value and less decrease in SC at high scan rates are expected for s-MnO_2.

Table 1
The estimated charges density at very low and very high sweep rate, and real charge density at 2 mV s^{-1} of both samples

	q_0 (C g^{-1})	q_T (C g^{-1})	q_r (C g^{-1})	q_0/q_T (%)	q_r/q_T (%)
s-MnO_2	156.8	295.2	246.2	53.2	83.4
co-MnO_2	27.7	212.8	146.5	13.0	68.8

The electrode of s-MnO_2 was subjected to galvanostatic charge–discharge cycling between −0.5 and 0.5 V versus Hg/Hg_2SO_4 in 1 mol L^{-1} Na_2SO_4 solution at a current density of 4.2 mA cm^{-2}. Typical curves of potential variation during the beginning three cycles with time of cycling are shown in Fig. 9. There is a linear variation of potential during charging and discharging processes, which is another criterion for capacitance behavior of a material in addition to exhibiting rectangular voltammograms. Fig. 9 shows that the time of charge and discharge are almost the same, which implies high reversibility and high Coulombic efficiency. The SC are calculated from galvanostatic charge–discharge cycling using the following equation

$$SC = \frac{It}{\Delta V m} \quad (5)$$

Where I is charge or discharge current, t is charge or discharge time, m is the mass of active material, and ΔV is potential window of cycling. Discharge SC obtained from second cycle is 219.7 F g^{-1}. The Coulombic efficiency is about 98% for all cycles.

An electrode made of s-MnO_2 was subjected to an extended charge–discharge cycling at a current density of 3.5 mA cm^{-2} and the result is shown in Fig. 10. After 600 cycles, only 6% decrease of SC was found, which shows good cycling properties of s-MnO_2.

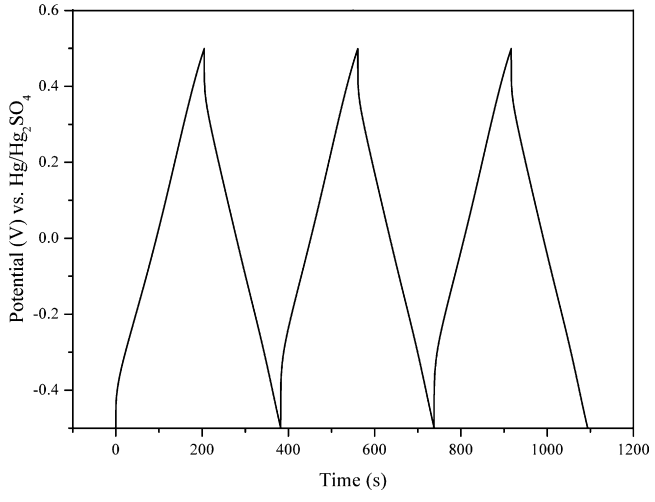

Fig. 9. Charge–discharge curves of s-MnO_2 at current density of 4.2 mA cm^{-2}.

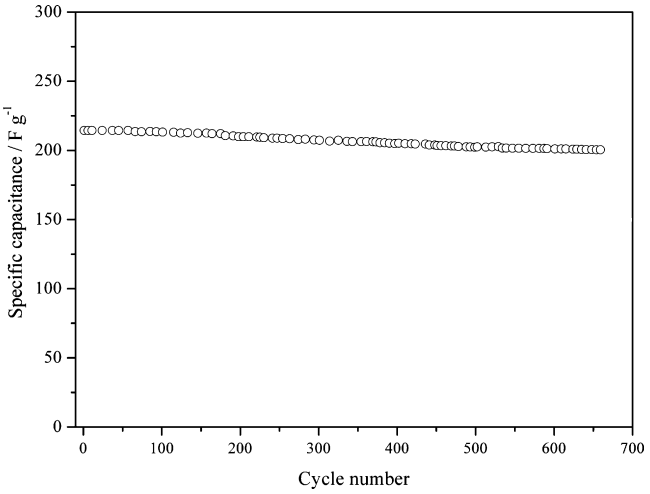

Fig. 10. Cycle-life data of s-MnO at 3.5 mA cm^{-2}.

4. Conclusion

Nanostructured hydrous manganese dioxide was prepared by a new simple method. $KMnO_4$ aqueous solution was dispersed in iso-octane by surfactant AOT and then $KMnO_4$ was reduced by AOT to produce MnO_2. The particles of MnO_2 are about 4 nm in diameter, which is much smaller than that of MnO_2 prepared by a chemical co-precipitation. A SC value as high as 246.2 F g^{-1} at 2 mV s^{-1} in 1 mol L^{-1} Na_2SO_4 solution was obtained. Deceasing in three-dimensional particle size will increase the outer surface area dramatically and improve the utilization of MnO_2, which is shown to be an efficient way to improve electrochemical properties of MnO_2 electrode for high-power supercapacitors applications.

Acknowledgements

This work was supported by the Natural Science Foundation of China under Grant No. 50632040. The authors would like to appreciate SAE Magnetic Ltd. for their supports on TEM and FT-IR measurements, and Prof. Ruowen Fu and Dr. Dingcai Wu from Sun Yat-Sen University for their help on the specific surface area measurements.

References

[1] B.E. Conway, Electrochemical Supercapacitors, Kluwer-Plenum, New York, 1999.
[2] J.P. Zheng, Electrochem. Solid-State Lett. 2 (1999) 359–361.
[3] H.Y. Lee, J.B. Goodenough, J. Solid State Chem. 144 (1999) 220–223.
[4] T. Brousse, M. Toupin, R. Dugas, L. Athouël, O. Crosnier, D. Bélanger, J. Electrochem. Soc. 153 (2006) A2171–A2180.
[5] R.N. Ready, R.G. Ready, J. Power Sources 132 (2004) 315–320.
[6] V. Subramanian, H.W. Zhu, B.Q. Wei, J. Power Sources 159 (2006) 361.
[7] A. Zolfaghari, F. Ataherian, M. Ghaemi, A. Gholami, Electrochim. Acta 52 (2007) 2806–2814.
[8] T. Xue, C.-L. Xu, D.-D. Zhao, X.-H. Li, H.-L. Li, J. Power Sources 164 (2007) 953–958.
[9] C.-C. Hu, T.-W. Tsou, Electrochem. Commun. 4 (2002) 105–109.
[10] C.-C. Hu, C.-C. Wang, J. Electrochem. Soc. 150 (2003) A1079–A1084.
[11] J.N. Broughton, M.J. Brett, Electrochim. Acta 50 (2005) 4814–4819.
[12] K.R. Prasad, N. Miura, J. Power Sources 135 (2004) 354–360.
[13] J. Wei, N. Nagarajan, I. Zhitomirsky, J. Mater. Process. Technol. 186 (2007) 356–361.
[14] Y.-T. Wu, C.-C. Hu, J. Electrochem. Soc. 151 (2004) A2060–A2066.
[15] C.Y. Lee, H.M. Tsai, H.J. Chuang, S.Y. Li, P. Lin, T.Y. Tseng, J. Electrochem. Soc. 152 (2005) A716–A720.
[16] N. Nagarajan, H. Humadi, I. Zhitomirsky, Electrochim. Acta 51 (2006) 3039–3045.
[17] S. Devaraj, N. Munichandraiah, J. Electrochem. Soc. 154 (2007) A80–A88.
[18] A. Yuan, Q.L. Zhang, Electrochem. Commun. 8 (2006) 1173–1178.
[19] M. Hibino, H.S. Zhou, I. Honma, J. Power Sources 146 (2005) 304–309.
[20] S. Ardizzone, G. Frengonara, S. Trasatti, Electrochim. Acta 50 (1990) 263–267.
[21] S. Wen, J.-W. Lee, I.-H. Yeo, J. Park, S.-iL Mho, Electrochim. Acta 50 (2004) 849–855.